Total electron scattering cross section from pyridine molecules in the energy range 10-1000 eV

A. Traoré Dubuis,[a] F. Costa,[a] F. Ferreira da Silva,[b] P. Limão-Vieira,[b] J. C. Oller,[c] F. Blanco,[d] and G. García[a]

[a] *Instituto de Física Fundamental, Consejo Superior de Investigaciones Científicas, Serrano 113-bis, 28006 Madrid, Spain*

[b] *Laboratório de Colisões Atómicas e Moleculares, CEFITEC, Departamento de Física, Universidade NOVA de Lisboa, 2829-516 Caparica, Portugal*

[c] *Centro de Investigaciones Energéticas, Medioambientales y Tecnológicas, 28040 Madrid, Spain*

[d] *Departamento de Física Atómica, Molecular y Nuclear, Universidad Complutense de Madrid, Avenida Complutense, 28040 Madrid, Spain*

ABSTRACT

We report on experimental total electron scattering cross-section (TCS) from pyridine (C_5H_5N) for incident electron energies between 10 and 1000 eV, with experimental uncertainties within 5-10 %, as measured with a double electrostatic analyser apparatus. The experimental results are compared with our theoretical calculations performed within the independent atom model complemented with a screening corrected additivity rule (IAM-SCAR) procedure which has been updated by including interference effects. A good level of agreement is found between both data sources within the experimental uncertainties. The present TCS results for electron impact energy under study contribute, together with other scattering data available in the literature, to achieve a consistent set of cross section data for modelling purposes.

Corresponding author:
G. García
Tel.: +34 91 5616800
Fax: +34 91 5854894
Email: g.garcia@csic.es

1. Introduction

Modelling radiation damage at the molecular level has recently motivated numerous studies on electron scattering from biologically relevant molecules [1]. In the last few years, special attention has been devoted to pyrimidine [2-8] ($C_4H_4N_2$) and its isomers (pyrazine [9] and pyridazine [10]) both in the gas and condensed phases as models for the pyrimidine nucleobases: thymine, cytosine and uracil. In particular, pyridine (molecular structure shown in Fig. 1) has recently been studied in terms of electron scattering cross section calculations for elastic and inelastic processes, over a broad energy range, from 1 to 1000 eV [11], by combining the R-Matrix method [11, 12] for the lower energies with the IAM-SCAR approach [13, 14] for intermediate and high energies. Low-energy electron scattering from pyridine has also been investigated by Barbosa et al. [15] using the Schwinger Multichannel Method (SMC) with pseudopotentials [16]. Electron impact ionisation cross sections were measured by Jiao et al. [17] and Bull et al. [18]. Electron transmission spectroscopy (ETS) experiments on pyrimidine have been performed by Modelli and Burrow [18] and Nenner and Schulz [20] together with other pyridine and azabenzene compounds. In the low-energy region, below 10 eV, comparison between theory and experiment allowed the characterization of low-lying resonances. These studies provided a reasonably accurate set of differential and integral elastic cross section data ready to be used for modelling electron tracks. Moreover, such achievement permits to evaluate transport properties in biologically relevant media, similar to the work performed by de Garland et al. [21] in tetrahydrofuran. A comprehensive review on electron scattering data required by such models has recently been published by Brunger [22]. However, to our knowledge, no experimental total scattering cross sections on electron scattering from pyridine for energies above 10 eV are available in the literature. In order to obtain a consistent set of cross section data for modelling purposes, the total electron scattering cross section (TCS) is one of the most relevant parameters. Note that these models require knowing such parameters over a broad energy range, in principle from the high incident energy of primary particles down to their final thermalisation in the medium (See Ref. [1] and references therein). From the experimental point of view, absolute TCS values can be determined with typical uncertainty limits within 5-10 % and, being the sum of all the accessible collision processes at a given energy (open channels), they constitute reference values to check the consistency of the available scattering cross section data.

In this study we present experimental total electron scattering cross sections from pyridine as measured with a double spectrometer electron transmission apparatus [23]. Our previous IAM-SCAR calculation has also been updated by including interference effects [24] and the new theoretical results are compared against previous calculations and the present experimental

values.

2. Experiment

2.1. Experimental set-up and procedure

The experimental setup has been described in detail elsewhere [23] and we will only report here a brief description. A schematic diagram of the experimental setup is shown in Fig. 2. Basically, it is a transmission beam experiment using a double electron spectrometer arrangement to reduce the electron beam energy spread and to analyse the energy distribution of scattered electrons. The electron beam is generated by a thoriated-tungsten hairpin filament coupled to a hemispherical electron monochromator. The primary beam, typically with 100 meV energy spread, is deflected and then focused into the entrance aperture of the scattering chamber (SC). The SC consist of a 50x50x50 mm^3 metallic (Dural) cube defined by a pair of 2 mm diameter apertures separated by a 50 mm length (*L*). Perpendicularly, a 32 mm diameter polytetrafluoroethylene (PTFE) tube connects the chamber with the gas inlet and the MKS-Baratron (627B) absolute capacitance manometer, so maintaining a steady gas flow during the measurements. Electrons emerging from the SC are analysed in energy with the second hemispherical spectrometer and finally detected with a two stage microchannel plate (MCP) operating in single counting mode.

The monochromator, collision chamber and analyser regions are differentially pumped by three turbo-pumps which allow reaching a background pressure of about 10^{-8} Torr. This pumping scheme allowed maintaining the pressure in the monochromator and analyzer regions below 10^{-7} Torr during the measurements while the pressure in the scattering chamber was varied between 0.1 and 5 mTorr.

The observed intensity follows the well-known attenuation (Beer-Lambert) law

$$I = I_0 \exp(-nl\sigma_{tot}), \qquad (1)$$

where I_0 is the intensity of the primary electron beam, *I* is the transmitted intensity in the forward direction and σ_{tot} is the total electron scattering cross section. l represents the interaction region length which we assume is coincident with the SC geometrical length (*L*), and *n* is the molecular density of the target.

For the molecular density value, n_e, at which the initial intensity is attenuated by a factor *e*, $I = I_0 / e$, being *e* the Euler's number, the total scattering cross section can be derived from:

$$\sigma_{tot} = \frac{1}{n_e l} = \frac{CT}{P_e L} \qquad (2)$$

where we are assuming an ideal gas behaviour of the target (P_e and T are the pressure and temperature measurements corresponding to the n_e molecular density). L represents the geometrical length of the scattering chamber and $C=\alpha k$ is a constant which includes the Boltzmann constant (k) and a correction factor (α) which accounts for possible systematic errors arising from the measured P and L values. Note that the differential pumping system used in this experiment does not ensure that the actual absorption length (l) corresponds to the measured geometric length (L) and some pressure gradient between the pressure gauge position and the interaction region may appear. T is derived from $T = \sqrt{T_c T_m}$, where T_c and T_m are the temperature of the scattering chamber measured with a thermocouple and the Baratron gauge operating temperature.

Another relevant feature of the apparatus is the angular acceptance of the hemispherical spectrometer used as energy analyser of the transmitted electrons. The 1.5 mm width entrance aperture of the monochromator is placed at 400 mm from the centre of the SC. Under these conditions, the solid angle subtended by the detector is of the order 10^{-5}sr leading to a practical acceptance angle of about 0.25 deg.

The analyser was remotely controlled by a PC running suitable custom LabView (National Instruments) program in order to record the EEL spectra and the attenuation of the primary beam as a function of the gas pressure in the SC. Using this data the LabView program provided the attenuation plots and the corresponding TCS results. For a given incident energy, at least 10 points of pressure were considered for each attenuation plot. Each cross section measurement was repeated at least three times so assuring statistical uncertainties below 10%.

The overall energy resolution was determined by looking at the nearest distinguishable features of the EEL spectra from nitrogen gas. The best resolution was found to be $\sim$0.5 eV.

The pyridine liquid sample used in the experiment was purchased from Sigma-Aldrich with a minimum purity of 99%. Air was removed from the sample by a repeated freeze–pump–thaw cycle using liquid nitrogen. Nevertheless, before taking any measurement, we monitored the quality of the sample by recording electron energy loss spectra to perform a qualitative analysis of the target in order to guarantee the absence of nitrogen or any other contaminant. A typical electron energy loss spectrum is shown in Fig. 3 for 609 eV incident electron energy and 3 mTorr of pyridine in the SC. The two inelastic peaks below 10 eV shown in Fig. 3 correspond to the electronic excitation of pyridine bound states whilst the broad structure above 10 is due to ionising collisions. As shown in this figure, the energy resolution used in this experimental study is good enough to distinguish any electronic excitation of the target within the transmitted beam

intensity.

2.2. Experimental uncertainties

The accuracy of pressure measurements is assumed to be better than 1% referring to manufacturer data sheet (MKS Baratron). The collision chamber is assumed to be at room temperature with an uncertainty of 1%. The incident beam energy given by a Bertan power supply, exhibiting a maximum standard deviation of 1 eV as measured by a Keithley 6517A electrometer. This results on an uncertainty of about 10% on the reported TCS value at 10 eV electron energy, and less than 0.2% above 500 eV. The experimental reproducibility of the results lies between 1.5% and 10%.

A source of systematic errors in such an apparatus results from electrons emerging in the forward direction due to elastic scattering and rotational and vibrational excitations of the ground state. In fact, Eq. (1) assumes an infinitely narrow electron beam and a null detector solid angle. The effect of the 0.25º acceptance angle is lowering the measured TCS and its magnitude is discussed in section 4.

Combining the above random uncertainty sources, their contributions to the total uncertainty limits of the present experimental TCSs are about 3% for the incident energy range considered. This percentage encompasses other sources of errors such as temperature variation, uncertainty in the curve fitting process and filament current.

Due to the geometry of the present experiment, other sources of systematic errors are connected with the assumption that the actual absorption length (l in equation (1)) is coincident with the geometrical length of the scattering chamber (L in equation (2)) and with possible pressure gradients between the electron interaction region and the Baratron gauge position which may be originated by the differential pumping system. For a proper evaluation of the influence of these systematic error sources in the experimental values, measurements should be repeated with different scattering geometries and measuring the pressure closer to the electron beam pathway. The rigid configuration of the present experimental setup did not allow these to be implemented but as the effect of both factors must be proportional, represented by the α factor defined above, we decided to measure the electron scattering TCS for a well-known target, as is the case of Argon. Results for selected incident energies (133, 174 and 244 eV) were compared with those recommended in a recent review from Gargioni and Grosswendt [25], obtaining TCS values systematically lower by 15%. A corrective factor derived from these effects results in a value of α=1.15±0.03 that was then included in equation (2) to derive our TCS values.

By combining all random uncertainty sources, the total uncertainty limits range from 3.3 to 10% depending on the incident electron energy with the maximum value found for 902 eV impact energy.

3. Theoretical calculations

As already mentioned in a previous study [11], we used our independent atom model with the screening corrected additivity rule (IAM-SCAR) procedure to calculate the differential and integral elastic as well as integral inelastic electron scattering cross sections from pyridine for impact energies between 0.1 and 1000 eV. Details on this calculation can be found in Ref. [11]. In a recent publication [24], we established the relevance of interference terms in the calculation of both differential and integral elastic cross sections for polyatomic molecules. We have therefore recalculated here the scattering processes studied in Ref. [11] through the IAM-SCAR method but including the interference terms as indicated in Ref. [24] by means of the so called IAM-SCAR+I procedure. Briefly, the molecular scattering amplitude is derived from the common expression for multicentre dispersion:

$$F(\theta) = \sum_{atoms} f_i(\theta) e^{i\mathbf{q}\cdot\mathbf{r}_i} \qquad (3)$$

Here, $\mathbf{q} = \mathbf{k}_{out} - \mathbf{k}_{in}$ is the momentum transfer, $\mathbf{r}_i$ are the atomic positions and $f_i(\theta)$ are the atomic scattering amplitudes. By averaging the squared modulus, $|F(\theta)|^2$, for all the molecular orientations, the differential elastic cross sections are derived according to:

$$\frac{d\sigma^{elastic}_{molecule}}{d\Omega} = \sum_{i,j} f_i(\theta) f_j^*(\theta) \frac{\sin qr_{ij}}{qr_{ij}} = \sum_i |f_i(\theta)|^2 + \sum_{i \neq j} f_i(\theta) f_j^*(\theta) \frac{\sin qr_{ij}}{qr_{ij}} =$$

$$\sum_i \frac{d\sigma^{elastic}_{atom\ i}}{d\Omega} + \frac{d\sigma^{interference}}{d\Omega} \qquad (4)$$

where $q \equiv |\mathbf{q}| = 2k \sin \theta/2$, r_{ij} is the distance between i and j atoms, $\sin qr_{ij} / qr_{ij} = 1$ when qr_{ij}=0, and $d\sigma^{interference}/d\Omega$ represents the $\Sigma_{i \neq j}$ interference contribution to the molecular differential cross section.

By integrating equation (3), the integral elastic cross sections are given by:

$$\sigma^{elastic}_{molecule} = \sum_{atoms} \sigma^{elastic}_{atom\ i} + \sigma^{interference} \qquad (5)$$

where $\sigma^{interference}$ represents the integration of the differential interference contribution. In spite of the oscillatory nature of the interference terms, their main effect is to increase the scattering amplitudes for the smaller angles and therefore their overall contribution to the integral cross sections tends to increase the integral cross section values.

As described in previous contributions [13, 14], the above atomic scattering amplitudes are calculated through a complex optical potential whose imaginary part provides the corresponding integral inelastic cross sections by considering inelastic processes as absorptions from the incident electron beam.

As the above expressions correspond to the independent scattering from each atom, they are only valid for large interatomic distances compared to the wavelength associated to the incident electron projectile, i.e. for relatively high incident energies (typically above 100 eV). In order to extend its validity down to lower energies (around 10 eV) we introduced some screening coefficients (s_i) which reduce the contribution of each atom to the total molecular cross section ($0 \leq s_i \leq 1$). Details on the calculation of these coefficient can be found in Blanco and García [13, 14].

Thus, molecular total electron scattering cross sections can then be represented as a function of the atomic total scattering cross sections, the screening coefficients and the integrated interference terms as follows:

$$\sigma_{molecule}^{total} = \sum_{atoms} s_i \sigma_{atom\ i}^{total} + \sigma^{interference} \qquad (6)$$

More information about the calculation method summarized here together with details to calculate all the above magnitudes can be found in Refs. [13, 14, 24].

Concerning the uncertainties assigned to the present calculation, we can estimate some uncertainty limits by comparison with reliable differential and integral cross section measurements. In assertion of the validation procedure between theory and experiment, we have applied in different occasions the IAM-SCAR method to a large number of polyatomic molecules (see for example Hoshino et al. [26] and references therein). From the comprehensive comparison we can conclude that our calculated integral cross sections are generally reliable within 10% for incident energies ranging from 20 to 1000 eV. Differential cross sections also agree with the experimental values within 10% for small and large angles whereas for intermediate angles (30-50 degrees) discrepancies are found at about 25%, depending on the target molecule.

The key feature behind the IAM-SCAR+I method is that with only the atomic potentials and the atomic spatial coordinates, one can predict the molecular cross section with reasonable accuracy over a wide energy range, i.e. from approximately 20 eV up to 10 keV.

In addition, we have performed an independent calculation of the dipole-rotational excitation cross section within the framework of the Born approximation. Details on this calculation can be found in Ref. [11]

4. Results and discussion

The total electron scattering cross sections as measured with the experimental arrangement

described above are shown in Table 1 together with their estimated uncertainty limits, typically between 3.3 and 10%, depending on the incident energy.

To facilitate the discussion, our measurements are also plotted in Fig. 4. As far as authors are aware, no previous experimental TCSs have been found in the literature to compare with the present data with the exception of our previous calculation [11]. The present theoretical updated results including interference terms (IAM-SCAR+I) and those obtained by adding the rotational excitation cross sections (IAM-SCAR+I+R) have also been plotted in this figure for comparison. A close inspection of Fig. 4, shows that our measurements agree, within the combined uncertainty limits, with our updated calculation although experimental values tend to be systematically lower than the theoretical prediction. Comparing the present calculation with the previous of Ref. [11] in which interference terms were not included, we can see that, as expected from equation (5), the effect of these terms is to increment the integral elastic cross section and consequently the total scattering cross section. The magnitude of this enhancement increases with energy and is of the order of 30% for about 1000 eV. In the case of pyridine, a clear increment of the calculated TCS below 15 eV results when interference effects are included (see Fig. 4). This increment is confirmed by the present TCS measurement at 13 eV. For the lower energies we also plotted the Born-corrected R-Matrix calculation [7] which confirms the relevance of the interference terms.

Furthermore, comparing with the calculation including rotational excitations (IAM-SCAR+I+R) we found that these theoretical values tend to be larger than the experimental data by about 20-40%. In the case of pyridine the average rotational excitation energy is about 1 meV which is well below the 0.5 eV energy resolution of our analyser. In addition, dipole rotational processes tend to scatter electrons in the forward direction. If they are scattered into the 0.25^{o} acceptance angle of the analyser, the MCP detector will consider them as “unscattered” electrons, so lowering the measured TCS. To this effect also contributes electrons elastically scattered into the acceptance angle. As shown in Fig. 4, if we integrate the differential elastic and rotational excitation cross sections from 0.25 to 180^{o}, we obtain results in reasonable good agreement with the present experiment. We have found that the contribution of this systematic error to the measured TCS depends on the incident energy, varying from 0.2 % at 1000 eV to 10.5 % at 10 eV. Vibrational excitation of the ground state may also contribute to this effect but, in the energy range considered here, we can expect a small contribution from this inelastic channel and that has been neglected.

To better understand the cross section dependence upon the interference effects, we have compared both sets of calculations at the elastic differential cross section (DCS) level. We have plotted in Fig. 5 the calculated DCS for pyridine at 30 eV, with (IAM-SCAR+I) and without (IAM-

SCAR) interference terms. As can be seen in this figure, the SCAR+I differential cross section values are clearly more prominent for small scattering angles while for intermediate and large scattering angles differences are not so relevant. A similar behaviour was found for all the energies considered here. This obviously affects the integral elastic cross section which increases about 43% when interference terms are included in the calculation. Note that, for increasing energies, these differences could not be distinguished experimentally as most of the setups for DCS measurements do not discriminate such contribution for small scattering angles, typically below 10 degrees. For example, for incident energies of 500 eV (within the energy range considered in this study) the electron intensity scattered in the 0-10^{o} angular range represents more than 95% of the total electron scattered intensity. This minimum scattering angle depends on the experimental conditions and is limited by possible contamination with the primary beam. In fact, integral cross sections derived from the integration of measured DCS are not fully experimental. They require some theoretical approaches to extrapolate the experimental data to the smaller scattering angles. An interesting review on extrapolation methods based on the Born approximation has recently been reported by Tanaka et al. [21].

5. Conclusions

We report measurements on pyridine total electron scattering cross sections for impact energies between 10 and 1000 eV. To our knowledge, no previous experimental TCS data has been reported in the literature. These results are very important for modelling radiation effects where TCSs are considered as reference values. For the same energy range we have calculated the differential and integral elastic as well as integral inelastic and total electron scattering cross sections from pyridine by using our updated independent atom model with screening corrections including interference effects (IAM-SCAR+I) procedure. We have found a good agreement, within the estimated uncertainty limits, between our experimental and theoretical TCS results, being better when interference terms are included. The effect of the incorporated interference terms has been discussed by comparing the elastic differential scattering cross sections calculated either including or not these terms. We have shown that these mainly affect the forward scattering amplitudes which are clearly enhanced because of these interferences. This enhancement in the case of pyridine leads to an increment of the integral elastic cross section, typically of the order of 30%. We noted that, due to forward angle limitations, these interference effects are not clearly appreciable in the experimental apparatus customary used for DCS measurements. This aspect should be carefully considered when comparing theoretical and experimental differential and integral elastic scattering cross sections.

Acknowledgements

We acknowledge the financial support received from the Spanish Ministerio de Economia y Competitividad (Project FIS2016-80440), the European Union Seventh Frame- work Programme (PEOPLE-2013-ITN-ARGENT Marie Curie project) under grant agreement no. 608163 and the European Union COST Action CM1301 (CELINA). FFS acknowledges the Portuguese National Funding Agency FCT-MCTES through researcher position IF-FCT IF/00380/2014 and together with PLV the research grant UID/FIS/00068/2013. This work was also supported by Radiation Biology and Biophysics Doctoral Training Programme (RaBBiT, PD/00193/2010); UID/Multi/ 04378/2013 (UCIBIO).

References

[1] G. García Gómez-Tejedor, and M. C. Fuss (eds.) Radiation Damage in Biomolecular Systems, (Springer: London, 2012).

[2] M. C. Fuss, A. G. Sanz, F. Blanco, J. C. Oller, P. Limão-Vieira, M. J. Brunger, G. García Phys. Rev. A 88 (2013) 042702.

[3] M. C. Fuss, L. Ellis-Gibbings, D. B. Jones, M. J. Brunger, F. Blanco A. Muñoz, P.Limão-Vieira, G. García, J. Appl. Phys. 117 (2015) 214701.

[4] Z. Mašín, J. D. Gorfinkiel, D. B. Jones, S. Bellm, M. J. Brunger, J. Chem. Phys. 136 (2012) 144310.

[5] I. Linert, M. Dampc, B. Mielewska, M. Zubeck, Eur. Phys. D 66 (2012) 20.

[6] W. Wolff, H. Luna, L. Sigaud, A. C. Tavares, E. C. Montenegro, J. Chem. Phys. 140 (2014) 064309.

[7] W. Y. Baek, A. Arndt, M. U. Bug, H. Rabus, M. Wang, Phys. Rev. A 88 (2013) 032702.

[8] J. B. Maljković, A. R. Milosavljević, F. Blanco, D. Šević, G. García, B. P. Marinković Phys. Rev. A 79 (2009) 052706

[9] A. G. Sanz, M. C. Fuss, F. Blanco, J. D. Gorfinkiel, D. Almeida, F. Ferreira da Silva, P. Limão-Vieira, M. J. Brunger, G. García, J. Chem Phys. 139 (2013) 184310.

[10] L. Ellis-Gibbings, A. D. Bass, P. Cloutier, G. García, L. Sancke, Phys. Chem. Chem. Phys 19 (2017)13038.

[11] A. Sieradzka, F. Blanco, M. C. Fuss, Z. Mašín, J. Gorfinkiel, G. García,J. J. Phys. Chem. A 118 (2014) 6657.

[12] J. Tennyson, Phys. Rep. 491 (2010) 29.

[13] F. Blanco, G. García, Phys. Rev. A 67 (2003) 022701.

[14] F. Blanco, G. García, Phys. Lett. A 317 (2003) 458.

[15] A. S. Barbosa, D. F. Pastega, M. H. F. Bettega, Phys. Rev. A 88 (2013) 022705.

[16] K. Takatsuka, V. McKoy, Phys. Rev. A 24 (1984) 2473; 30 (1984) 1734.

[17] C.Q. Jiao , C.A. DeJoseph Jr., R. Lee , A. Garscadden, Int. J. Mass Spectrom 257 (2006) 34.

[18] J. N. Bull, J. W. L. Lee, C. Vallance, Phys. Chem. Chem. Phys. 16 (2014) 10743.

[19] A. Modelli, P Burrow, J. Electron Spectrosc. Relat. Phenom. 32 (1983) 263.

[20] I. Nenner, G. J. Schulz, J. Chem. Phys. 62 (1975) 1747.

[21] N. A. Garland, M. J. Brunger, G. García, J. de Urquijo, R.White, Phys. Rev. A 88 (2013) 062712.

[22] M. J. Brunger, Int. Rev. Phys. Chem. 36 (2017) 333.

[23] A.Traoré Dubuis, A. Verkhovtsev, L. Ellis-Gibbings, K Krupa, F. Blanco, D. B. Jones, M. J. Brunger, G. García, J. Chem Phys. 147 (2017) 054301.

[24] F. Blanco, L. Ellis-Gibbings, G. García, Chem. Phys. Lett. 645 (2016) 71.

[25] E.Gargioni, B. Grosswendt, Rev. Mod. Phys. 80 (2008) 451.

[26] M. Hoshino, P. Limão-Vieira, A. Suga, H. Kato, F. Ferreira da Silva, F. Blanco, G. García, H. Tanaka, J. Chem. Phys. 143 (2015) 024313.

[27] H. Tanaka, M. J. Brunger, L. Campbell, H. Kato, M. Hoshino, A. R. P. Rau, Rev. Mod. Phys. 88 (2016) 025004.

Table 1

Total cross section (10^{-20} m^2) measurements for pyridine as a function of the electron impact energy, statistical uncertainties and uncertainty limit. See text for details.

Energy (eV)	TCS (10^{-20} m^2)	Statistical uncertainty (%)	Uncertainty limit ($\pm10^{-20}$ m^2)
13	59.5	1.4	1.9
27	46.0	1.9	1.5
32	44.5	3.5	2.0
42	41.5	2.3	1.6
46	40.1	2.3	1.5
59	36.5	3.2	1.6
69	35.1	1.5	1.1
84	34.1	3.4	1.5
132	27.8	3.8	1.3
174	25.5	4.2	1.3
244	21.4	3.4	1.0
296	18.7	1.9	0.7
418	15.2	8.6	1.4
516	14.6	7.3	1.1
609	12.8	4.6	0.7
717	11.6	5.8	0.7
833	10.2	7.2	0.8
902	10.0	9.6	1.0

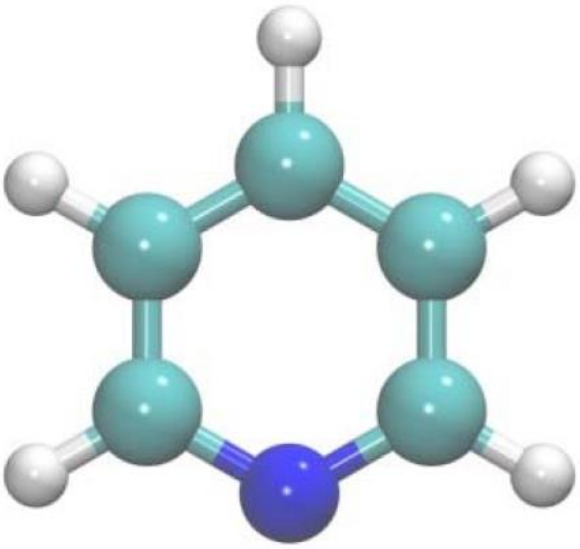

Fig. 1. Sketch of the pyridine (C_5H_5N) molecular structure. Carbon atoms are in green, hydrogen in white and nitrogen in blue

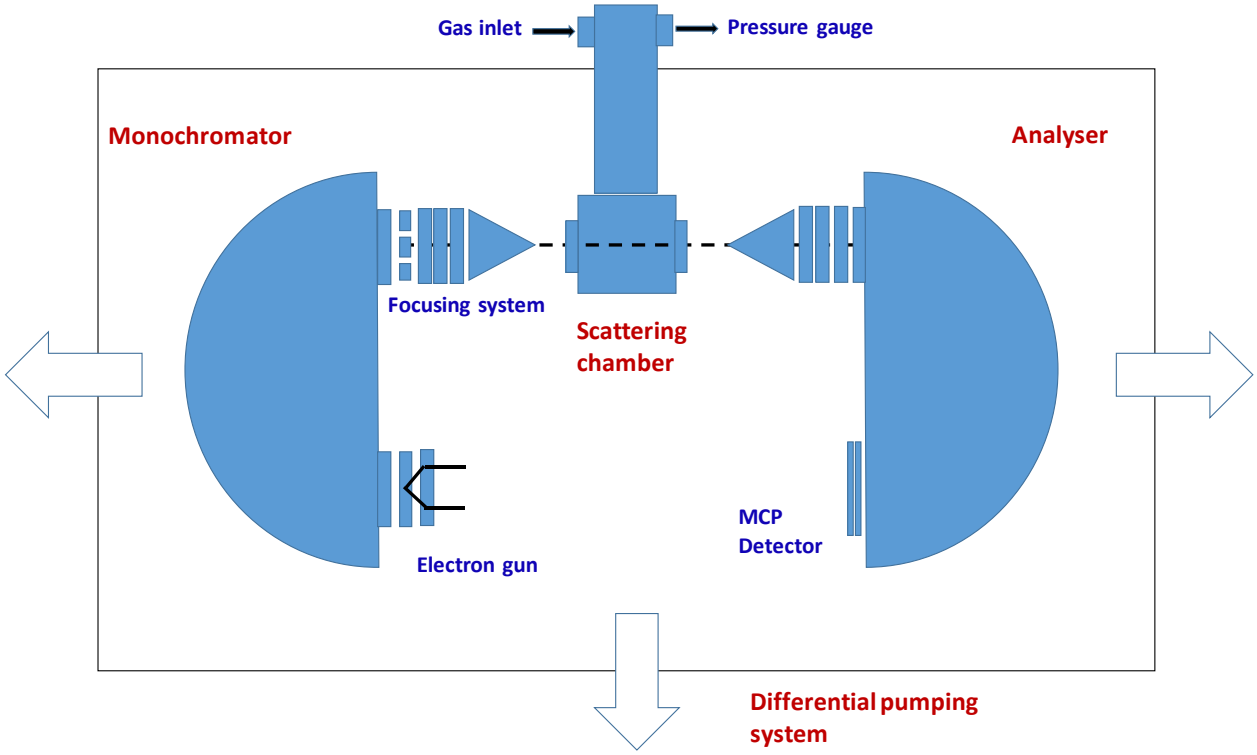

Fig. 2. Sketch of the double electrostatic analyzer used to perform the total cross section measurements from pyridine.

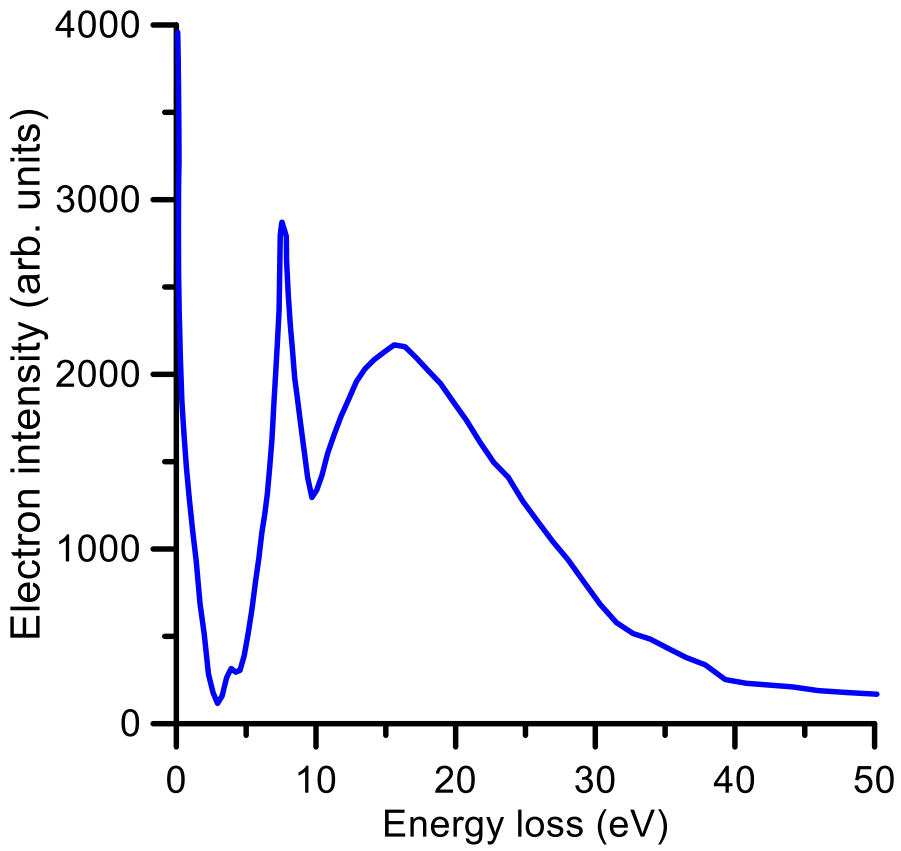

Fig. 3. Typical measured electron energy-loss spectrum at 609 eV incident electron with 3 mTorr of pyridine.

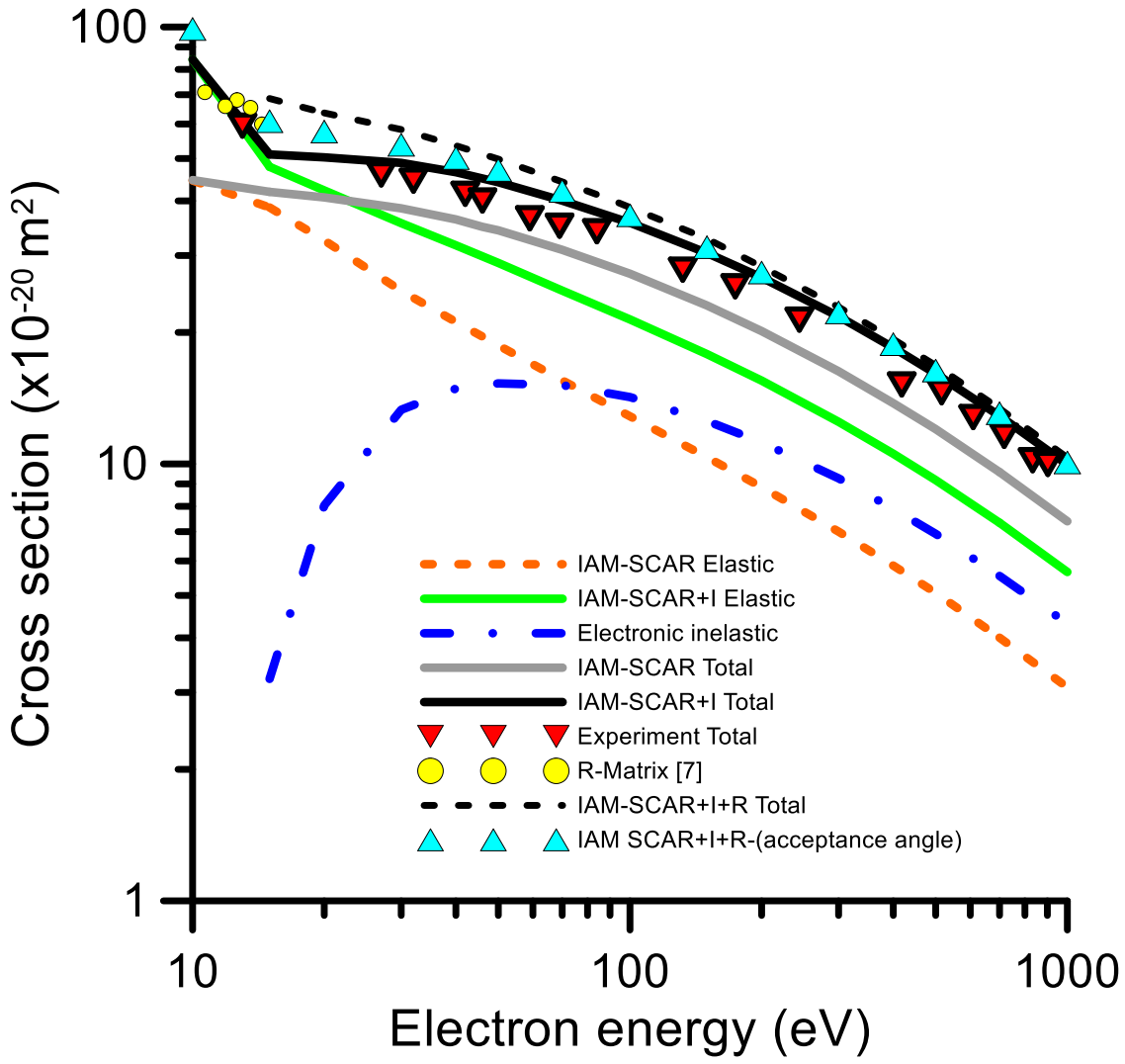

Fig. 4. Integral electron scattering cross sections from pyridine molecules (see text for details).

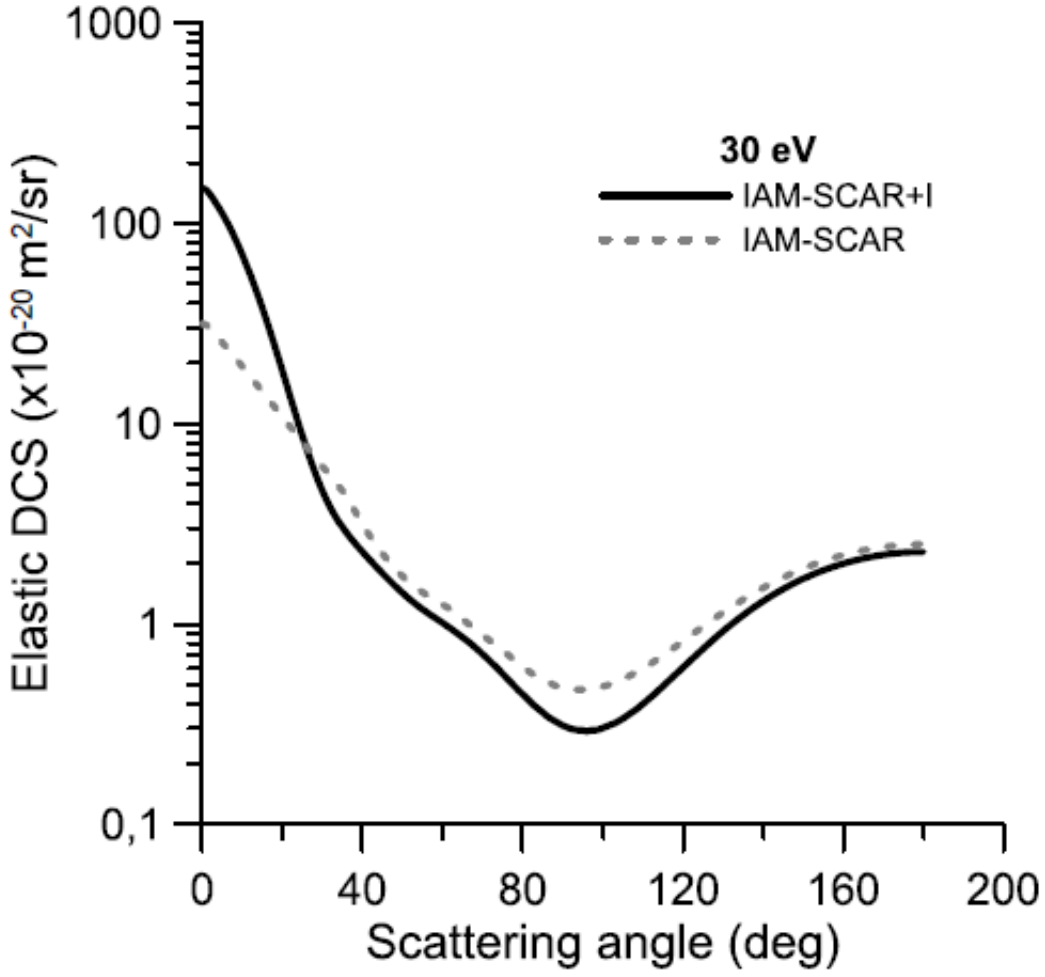

Fig. 5 Differential electron scattering cross section from pyridine for 30 eV incident electron energy.